A PREDICTION MODEL OF THE EFFECTIVE THERMAL CONDUCTIVITY OF THE MICRO-LATTICE PHASE CHANGE MATERIAL

Liang SHAN[1], Longquan LIU[1,*], Junming CHEN[2]

[*1]School of Aeronautics and Astronautics, Shanghai Jiao Tong University, Shanghai, China

[2]Shanghai Electro-Mechanical Engineering Institute, Shanghai, China

[*] Corresponding author; E-mail: liulongquan76@sjtu.edu.cn

Abstract: *The micro-lattice phase change material is a new type of thermal control material that effectively integrates the metallic hollow micro-lattice and phase change material together and exploits their advantages on the heat transfer capability and the heat storage capacity. This paper proposes a model to predict the effective thermal conductivity of micro-lattice phase change materials considering the heat transferring between the two different phases. The Fourier's law and the modified the volume calculation method were used to derive a new prediction model, and the prediction model was refined using the finite volume method. Testing and the finite element method were used to validate that the proposed prediction model is more accurate than traditional prediction models. At the same time, we also analyzed the influence of boundary effects and micro-structural parameters of the hollow micro-lattice on the effective thermal conductivity.*

Keywords: *hollow micro-lattice, effective thermal conductivity, phase change material*

1. Introduction

With the advancement of the aerospace industry, the demand for lightweight multifunctional materials that can be used to decrease the overall mass and volume while enhancing the reliability has become increasingly significant [1-3]. Owing to the use of highly integrated electronic devices, the heat generated during payload operation reduces the lifespan of the satellites [4]. Therefore, it is necessary to control the heat to improve overclocking reliability and extend product life [5, 6]. To overcome this challenge, there is an urgent need for multifunctional thermal control materials.

The various lightweight thermal control materials that have been developed so far include foams [7, 8], lattices [9], honeycombs [10], and corrugated material [11, 12]. Honeycomb and corrugated materials used in thermal control are typically filled with insulation or phase change materials for their intended use [13, 14]. Metal foam materials have the advantages of low density and a large specific surface area, and they have been widely used to enhance heat transfer [15]. Although foam materials possess certain advantages, their design limitations restrict their broader applications [16].

Lattice materials possess great potential for use in multifunctional applications due to their high porosity, specific stiffness, specific strength, specific surface area, and excellent design flexibility [17]. Hollow micro-lattice materials have been further explored as materials for thermal control [18, 19], An important parameter for evaluating the performance of thermal control materials is the estimation of the effective thermal conductivity. Qu *et al.* [20] divided the octet-truss lattice unit cell into several layers and calculated the thermal conductivity of each layer using the volume fraction, and then employed a series model to determine the overall effective thermal conductivity. Wang *et al.* [21] calculated the configuration factor by the Monte Carlo method, considering the influence of radiation in all directions. They also presented an analytical model for predicting the effective thermal conductivity of the pyramidal lattice core sandwich structure. Shiva *et al.* [22] investigated the thermal transport in hollow nickel micro-lattice and determined the effective thermal conductivity by analyzing the material's thermal characteristics, cell structure, and volume fraction.

Our team has conducted a series of researches on the application of micro-lattice materials for thermal control. Xu *et al.*[23] fabricated a hollow micro-lattice material embedded with phase change material, which is called micro-lattice phase change material. This material integrated the heat transfer capacity of lattice materials with the heat storage ability of phase change materials, and it was demonstrated to have excellent thermal control ability. Chen *et al.* [24] designed a new cooling system that utilizes a hollow metal micro-lattice material filled with liquid. This innovative design enhances heat dissipation performance while maintaining a lightweight structure. Subsequently, Chen *et al.* [4] conducted extensive research on hollow metal micro-lattice materials filled with phase change material. They analyzed the influence of microstructure features on the thermal control performance and simulated the thermal control effect under thermal load conditions of microsatellites.

In previous studies, the prediction of the thermal conductivity of lattice structures was primarily based on Professor Haydn N. G. Wadley's method [25]. However, there was a significant error in predicting the thermal conductivity of the micro-lattice phase change material. Therefore, a more accurate prediction model is necessary. In this study, a new prediction model was developed by using Fourier's law and modified volume calculation method. The modified parameters, calculated using the finite volume method, were used to modify the prediction model. The finite element and testing results have demonstrated that the prediction model proposed in this paper is more accurate than traditional prediction models, especially in limited size situations. Subsequently, we analyzed the effects of boundary effects and structural parameters on the effective thermal conductivity.

2. Structure of the micro-lattice phase change material

The structure of the micro-lattice phase change material studied is shown in Fig. 1. The overall structure consists of the representative unit repeated in a fixed array (Fig. 1(a)) The structure of the representative unit consisting twelve 45° circular rods is shown in Fig. 1(b).

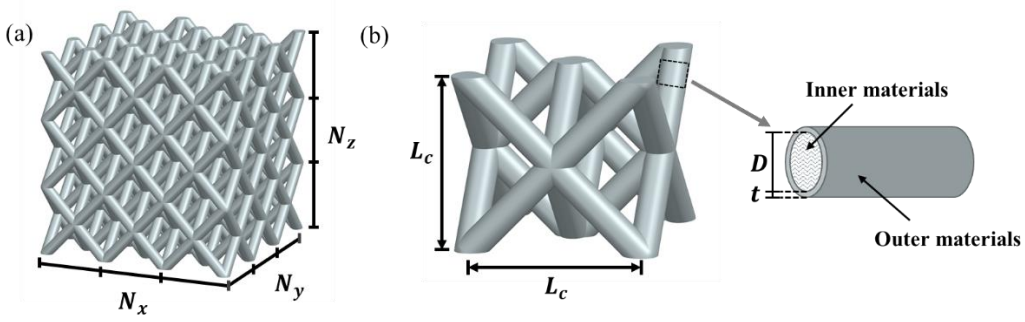

Figure 1. Microstructure of the micro-lattice phase change material.

The size of the representative unit is L_c, the number of representative units along the x, y and z directions are denoted as N_x, N_y and N_z, respectively, where z is the direction of heat transfer. Each rod is composed of inner materials made of phase change material with a diameter of D and the outer material made of metallic material with a thickness of t.

3. Prediction of the effective thermal conductivity

For the convenience of calculation, the two materials were considered as equivalent materials with a thermal conductivity of λ_s. The process of obtaining the effective thermal conductivity prediction model is shown in Fig. 2, the effective thermal conductivity of the solid lattice material was calculated first, and then the thermal conductivity of the heat transfer rod was calculated. From the results of the effective thermal conductivity of the solid lattice material and the thermal conductivity of the equivalent materials, it can be concluded that the prediction model for the effective thermal conductivity of the micro-lattice phase change material has been modified.

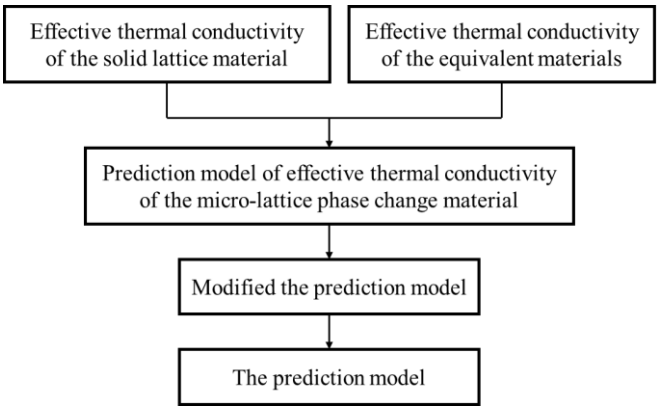

Figure 2. Calculation process of the effective thermal conductivity prediction model.

3.1. Effective thermal conductivity of the solid lattice material

Assuming the temperature difference at both ends of the lattice is ΔT, heat is transmitted along the direction of the rod, taking the representative unit as an example, the heat transfer path in the rods is shown in Fig. 3(b) and Fig. 3(c). A portion of the heat flow enters from a rod on the lower end face, and all short rods in the entire path of the upper end face are considered complete heat transfer rods, the thermal conductivity of the heat transfer rod is λ_s. According to Fourier's law, the number of heat transfer rods in the hole structure is

$$n = 8N_xN_y + 2(N_x + N_y)\#(1.)$$

The area of the end face is

$$S_b = (N_xL_c + D + 2t)(N_yL_c + D + 2t) \qquad (2.)$$

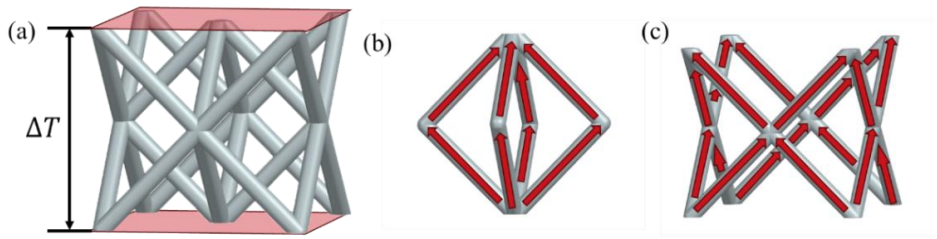

Figure 3. The heat transfer path of the lattice materials.

The heat conducted in the heat transfer rod and the equivalent body is

$$Q = -\lambda_s \frac{n\Delta T}{\sqrt{2}N_zL_c}\pi(R + t)^2 = -\lambda_{eff}\frac{\Delta T}{N_zL_c}S_b \qquad (3.)$$

The result can be obtained as

$$\lambda_{eff} = \lambda_s \frac{n\pi(R + t)^2}{\sqrt{2}S_b} \qquad (4.)$$

3.2. Effective thermal conductivity of the equivalent materials

In the case of using the lattice structure relative density calculation method [25], because the intersection part of the rods is not considered, the error will be unacceptable when the diameter is large. Therefore, we revised the volume calculation method.

3.2.1 Integral of the structural volume

The overall structure can be disassembled and divided into three parts as shown in Fig. 4(a). The beige part of the basic structure is a half cylinder with four corners cut off (Fig. 4(b)), while the green part of the basic structure is derived from the former by cutting off two intersecting 45° rods (Fig. 4(c)). The red part of the basic structure can be divided into two parts: one is the portion where the half cylinder is cut off (Fig. 4(d)), and the other is the portion where the hemisphere is cut off (Fig. 4(e)).

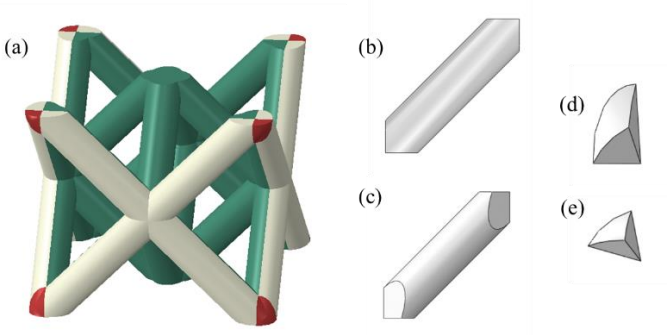

Figure 4. Schematic diagram of the lattice materials.

(1) Consider the beige part, compared to the semi-circular rod, four parts need to be cut along the reference plane, and the volume of the part cut along the base plane is

$$V_{beige} = \frac{\sqrt{2}L_c\pi R^2}{4} - \frac{4R^3}{3} \quad (5.)$$

(2) Consider the green part, The volume of the intersecting part is the volume of the frustum of two $45°$ circular rods (the angle between the two rods is $60°$). The volume of a frustum can be calculated using the formula:

$$V_{cut} = \int_0^{\sqrt{2}R}\int_0^{r^1} f(x,y)\,dx\,dy + \int_{\sqrt{2}R}^{\sqrt{3}R}\int_{r^2}^{r^1} f(x,y)\,dx\,dy \quad (6.)$$

with

$$f(x,y) = \sqrt{R^2 - \frac{(x-y)^2}{2}} - x;\ \ r^1 = \frac{y + \sqrt{6R^2 - 2y^2}}{3}, r^2 = \frac{y - \sqrt{6R^2 - 2y^2}}{3}$$

From this, the volume of the green part can be determined as

$$V_{green} = \frac{\sqrt{2}L_c\pi R^2}{4} - \frac{4R^3}{3} - 2V_{cut} \quad (7.)$$

(3) Consider the red part, $V_{red} = V_{red,1} + V_{red,2}$, the intersection bodies of the edge rods are distributed along the edges, the volume shown in Fig. 4(d) is

$$V_{red,1} = \frac{1}{\sqrt{2}}\int_0^{\sqrt{\frac{2}{3}}R}\int_{-\sqrt{R^2-\frac{y^2}{2}}}^{-y}\sqrt{2R^2 - 2x^2} - y\,dx\,dy \quad (8.)$$

The volume shown in Fig. 4(e) is

$$V_{red,2} = \int_0^{\frac{R}{\sqrt{3}}}\int_y^{\sqrt{\frac{R^2-y^2}{2}}}\sqrt{R^2 - x^2 - y^2} - x\,dx\,dy \quad (9.)$$

3.2.2 The volume function

The function of the total volume of the structure can be obtained from these equations as

$$V = f(N_x, N_y, N_z, L_c, R) = 8(N_xN_z + N_zN_y)V_{beige} + 32N_xN_yN_zV_{green} + 16N_zV_{red} \quad (10.)$$

For ease of calculation, use fitting results

$$8N_z(N_x + N_y)\left(\frac{\sqrt{2}L_c\pi R^2}{4} - \frac{4R^3}{3}\right) + 32N_xN_yN_z\left(\frac{\sqrt{2}L_c\pi R^2}{4} - 2.575R^3\right) + 1.6032N_z\pi R^3 \quad (11.)$$

By using the revised volume formula, we can obtain the true volumes of two materials.

$$V_{in} = f(N_x, N_y, N_z, L_c, R), V_{out} = f(N_x, N_y, N_z, L_c, R+t) - f(N_x, N_y, N_z, L_c, R) \quad (12.)$$

According to the parallel model, the effective thermal conductivity of the equivalent materials is

$$\lambda_s = \frac{V_{in}\lambda_{in} + V_{out}\lambda_{out}}{V_{in} + V_{out}} \quad (13.)$$

Then we can get the thermal conductivity of the micro-lattice phase change material

$$\lambda_{eff} = \left[\frac{f(N_x, N_y, N_z, L_c, R)}{f(N_x, N_y, N_z, L_c, R+t)}(\lambda_{in} - \lambda_{out}) + \lambda_{out}\right] \cdot \frac{n\pi(R+t)^2}{\sqrt{2}S_b} \quad (14.)$$

4. Modification of the prediction model

In finite element analysis and experiments, it has been observed that the simple structural accumulation in the direction of heat transfer can increase the effective thermal conductivity. This effect is particularly pronounced when there is only one representing unit in the direction of heat transfer. In practical applications, there is often only one or two layers of lattice in the direction of heat transfer. Modifying this situation can effectively improve the accuracy of predictions for practical applications.

Considering that the structure used in this paper was composed of internal and external parts. For this double-layer structure, *ABAQUS* may be used to establish the basic cylindrical rod model, similar to the previous study. A layer of shell elements was applied to the surface of the round rod, and the steady-state solution was conducted for various heat transfer lengths to calculate the effective thermal conductivity.

As shown in Fig. 5, the model exhibits a trend similar to that of the micro-lattice phase change material, indicating that this type of structure has an impact on the prediction of effective thermal conductivity. To minimize its impact, the finite volume method is employed to numerically compute the cylindrical model with an outer layer. The goal is to obtain a fitting formula that is related to the length of the heat transfer rod and utilize it as a modified coefficient for similar scenarios.

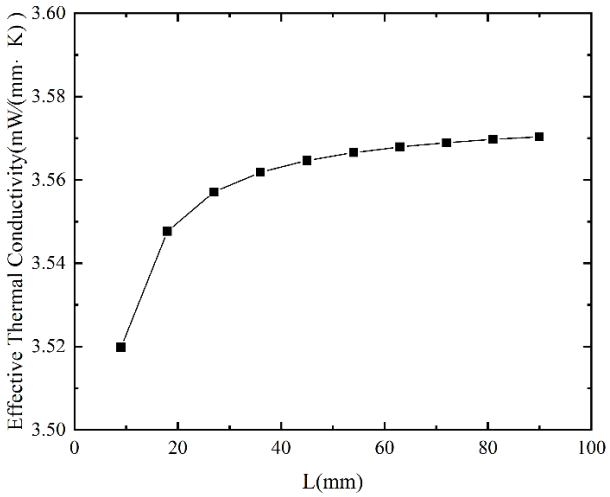

Figure 5. Effective thermal conductivity in cylinder with a layer of shell.

4.1. Finite Volume Method

The finite volume method was used to estimate the heat conduction of the double-layer cylinder. This method considers the temperature distribution in the double-layer cylinder for steady-state heat conduction analysis using the control differential equation. There was no internal heat generation, and the calculation was performed using an axisymmetric grid [26].

The structure is simulated using an axisymmetric model and the axisymmetric algorithm was used. As shown in Fig. 6(a), a cylindrical half section was employed as the calculation area, where adiabatic boundaries was set on both the left and right sides, while the interfacial heat transfer occurs between the two phases.

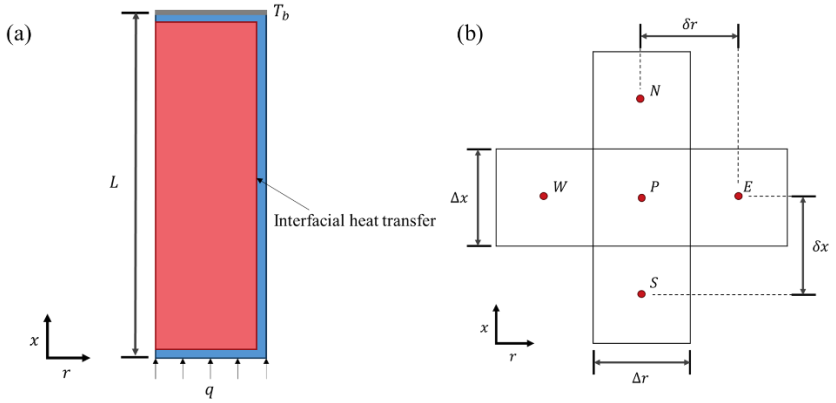

Figure 6. Finite volume method.

For the heat transfer process, the energy balance equation of the control volume is

$$Q_W + Q_E + Q_S + Q_N = 0 \quad (15.)$$

In the equation, Q_W, Q_E, Q_S and Q_N represent the heat quantity transferred to the control volume P from the adjacent nodes W, E, S and N, respectively through heat conduction (Fig. 6(b)). For the control volume P, the discretization equation of the energy governing equation is

$$a_P \cdot T_P^K = a_W \cdot T_W^K + a_E \cdot T_E^K + a_N \cdot T_N^K + a_S \cdot T_S^K + b \ (16.)$$

with

$$a_W = \frac{\lambda\left(r_P - \frac{\Delta r}{2}\right)\Delta x}{\delta r},\ a_E = \frac{\lambda\left(r_P + \frac{\Delta r}{2}\right)\Delta x}{\delta r},\ a_N = \frac{\lambda r_P \Delta r}{\delta x},\ a_S = \frac{\lambda r_P \Delta r}{\delta x}$$

$$a_P = a_W + a_E + a_N + a_S,\ b = b_1 + b_2$$

Taking into consideration the grid adjacent to the boundary in the solution domain. The coefficients corresponding to connected boundaries change under different boundary conditions. a_v is the corresponding coefficient, S_v is the corresponding contact surface area.

(1) Adiabatic boundary condition

$$a_v = 0 \quad (17.)$$

(2) Dirichlet boundary condition

$$a_W = \frac{2\lambda\left(r_P - \frac{\Delta r}{2}\right)\Delta x}{\delta r}, a_E = \frac{2\lambda\left(r_P + \frac{\Delta r}{2}\right)\Delta x}{\delta r}, a_N = \frac{2\lambda r_P \Delta r}{\delta x}, a_S = \frac{2\lambda r_P \Delta r}{\delta x}$$

$$b_1 = a_v \cdot T_b \ (18.)$$

(3) Neumann boundary condition

$$a_v = 0, b_2 = qS_v \quad (19.)$$

(4) Interfacial heat transfer

$$a_v = hS_v \ (20.)$$

Taking into account that the interfacial heat transfer between two materials has an upper limit, we utilized the harmonic mean of the thermal conductivity between the control points on either side of the interface [27].

$$\lambda_m = \frac{\Delta r_1 + \Delta r_2}{\frac{\Delta r_1}{\lambda_1} + \frac{\Delta r_2}{\lambda_2}} \quad (21.)$$

Therefore, a_v should not exceed

$$\frac{\lambda_m S_v}{\frac{\Delta r_1}{2} + \frac{\Delta r_2}{2}} \quad (22.)$$

4.2. Modified coefficient

In numerical calculations, the value of the Dirichlet boundary condition is T_b, the value of the Neumann boundary condition is q, heat transfer length L equals $N_z L_c$, and the average temperature of the bottom side is T_d. Therefore, the effective thermal conductivity of the cylindrical model is

$$\lambda_p = \frac{qL}{T_d - T_b} \quad (23.)$$

The effective thermal conductivity, calculated using the finite volume method under different grid sizes, was compared to that calculated using the *ABAQUS* axisymmetric model under the same conditions. It can be seen in Tab. 1, that the finite volume method exhibits good grid independence, and the relative error with *ABAQUS* is very small when the grid size reaches 0.01 mm. Excessively small grid sizes can significantly increase the computational workload. Therefore, in the subsequent calculations, the grid size was set to 0.01mm.

Table 1. Relative error comparison in different grid sizes.

Grid size (mm)	0.08	0.04	0.02	0.01	0.008	0.005	0.004	0.002	0.001
Relative error (%)	1.047	0.553	0.345	0.253	0.236	0.212	0.204	0.190	0.183

Taking 580608 sample points within the $R \in [0.35,1]$, $t \in [0.01,0.2]$, $\lambda_{in} \in [0.1,4]$, $\lambda_{out} \in [50,200]$, and $L \in [0.5,100]$ interval for calculation by using *MATLAB*. The following fitting relationship between various parameters and effective thermal conductivity is obtained:

$$\lambda_{eff} = \left(1 + k_1 \frac{R+t}{L}\right) \frac{R^2}{(R+t)^2} \lambda_{in} + \left(1 + k_2 \frac{R+t}{L}\right) \frac{2Rt + t^2}{(R+t)^2} \lambda_{out} + k_3 \frac{t^2}{L} + k_4 \frac{Rt}{L} \#(24.)$$

with

$$k_1 = 0.1245, k_2 = -0.0103, k_3 = 144.9565, k_4 = -26.8147$$

Histograms of the relative error distribution is shown in Fig. 7. The relative error of the vast majority of data is within 2%, and the mean-square error is 0.1793, which verifies that using this fitting equation as an alternative is acceptable.

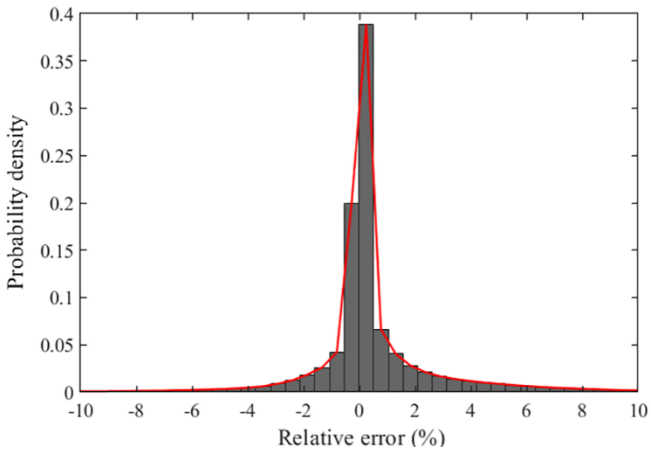

Figure 7. The relative error histogram of the fitting equation.

When the heat transfer length is infinite, the equation can be simplified as a mixing rule formula, so the adjustment coefficient can be considered as the ratio of this fitting formula to the mixing rule. Therefore, the modified coefficient can be calculated as bellow

$$\alpha = \frac{\left(1 + k_1 \frac{R+t}{L}\right)\frac{R^2}{(R+t)^2}\lambda_{in} + \left(1 + k_2 \frac{R+t}{L}\right)\frac{2Rt+t^2}{(R+t)^2}\lambda_{out} + k_3 \frac{t^2}{L} + k_4 \frac{Rt}{L}}{\frac{R^2}{(R+t)^2}\lambda_{in} + \frac{2Rt+t^2}{(R+t)^2}\lambda_{out}} \quad (25.)$$

When there is only one or two cells in the heat transfer direction, the effective thermal conductivity can be predicted by the following equation:

$$\lambda_{eff} = \alpha \left[\frac{f(N_x, N_y, N_z, L_c, R)}{f(N_x, N_y, N_z, L_c, R+t)}(\lambda_{in} - \lambda_{out}) + \lambda_{out}\right] \cdot \frac{n\pi(R+t)^2}{\sqrt{2}S_b} \quad (26.)$$

This prediction model is mainly aimed at limited size situations, as the influence of boundary effects is significant and should not be disregarded. When the size is large, i.e. N_x, N_y and N_z are large, we can ignore the influence of the boundary part. Under these conditions, the prediction model can be simplified as a homogenization prediction model:

$$\lambda_{eff} = \left[\frac{L_c R^2 - 2.3186R^3}{L_c(R+t)^2 - 2.3186(R+t)^3}(\lambda_{in} - \lambda_{out}) + \lambda_{out}\right] \cdot \frac{4\sqrt{2}\pi(R+t)^2}{L_c^2} \quad (27.)$$

5. Verification of the effective thermal conductivity prediction model

The thermal conductivity of Ni-P coating and octadecane at room temperature was obtained using a laser thermal conductivity meter (LFA467, Germany) with values 66.6 $Wm^{-1}K^{-1}$ and 0.17 $Wm^{-1}K^{-1}$ [4].

5.1. The effective thermal conductivity test setup

The test setup of the effective thermal conductivity measurement is shown in Fig. 8. The sample was assembled between quartz and stacked between the heat source and the fixed heat sink in a vacuum environment. The vacuum level inside the vacuum chamber was below $-0.8MPa$, and heat propagates from the bottom of the heater to the fixed heat sink.

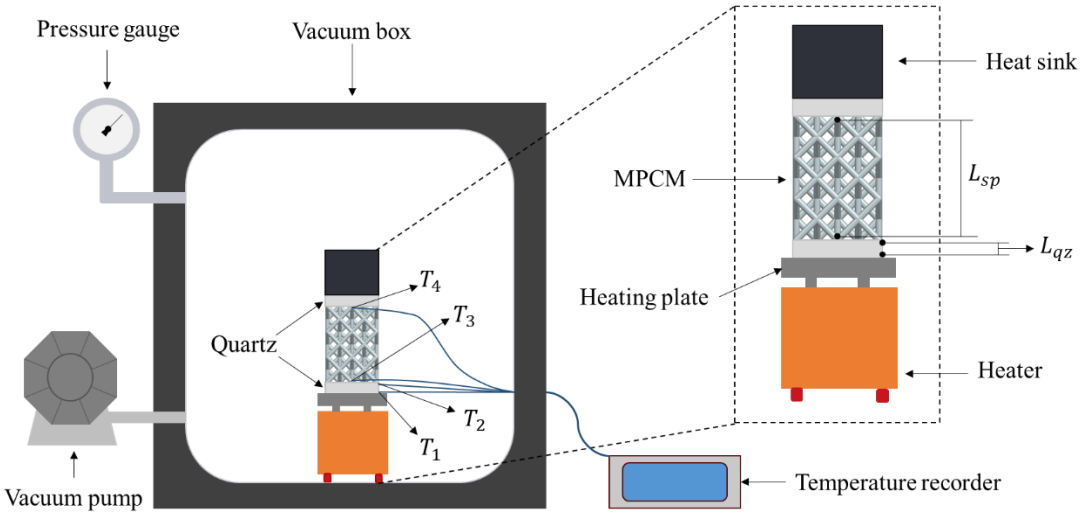

Figure 8. Test setup.

The temperatures at four points, two on the quartz and two on the sample, were measured using a thermocouple. A thermal conductivity analyzer (HotDisk TPS3500S, Sweden) was used, the thermal conductivity of quartz at room temperature was obtained to be 1.217 $Wm^{-1}K^{-1}$. The effective thermal conductivity of the sample was calculated by using the known thermal conductivity of quartz and the length between the thermocouple points. According to the reference literature [22] and simulations, the proportion of radiant heat transfer is extremely small at the set temperature.

For the quartz section and the sample section:

$$q_{test} = -\lambda_{qz}\frac{T_1 - T_2}{L_{qz}} = -\lambda_{eff}\frac{T_3 - T_4}{L_{sp}} \quad (28.)$$

Eq. (28) is reorganized and solved to obtain the effective thermal conduction:

$$\lambda_{eff} = \lambda_{qz}\frac{L_{sp}(T_1 - T_2)}{L_{qz}(T_3 - T_4)} \quad (29.)$$

5.2. Numerical model

As shown in the Fig. 9, a finite element model was established using the finite element code, *Abaqus/Standard*. Taking the $(N_x, N_y, N_z, L_c, R, t)$= $(2,2,1,5,0.5,0.02)$ and the inner phase change material was modelled using solid elements, the outer layer of metallic material was modelled using shell elements. Thermal contact was set between the inner and outer part, a constant temperature boundary conditions T_{up} was set on the upper end face, and a heat flux of q_{down} was set on the lower end face.

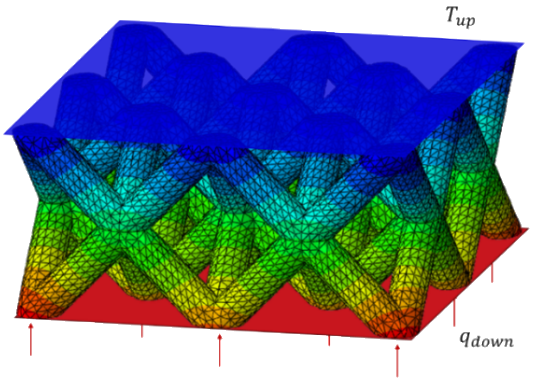

Figure 9. Finite element model setup.

The analysis was carried out using a steady-state heat transfer mode. The average value of the lower surface temperature was selected as T_{down}, and the effective thermal conductivity is

$$\lambda_{eff} = q_{down} \frac{N_z L_c}{T_{down} - T_{up}} \quad (30.)$$

In order to verify the accuracy of the numerical model, we conducted the experiments for comparison. To compare with experimental data, the temperature value of the numerical model corresponds to the attachment point of the experimental thermocouple, rather than the average temperature value of the surface. The structural parameters of the prepared samples are the same (N_x, N_y, L_c, R, t)= (2,2,9,0.75,0.02), except for the difference in N_z.

It can be seen in Fig. 10 that the results of the numerical model are consistent with the experimental results. Therefore, the numerical model presented in this article is reliable.

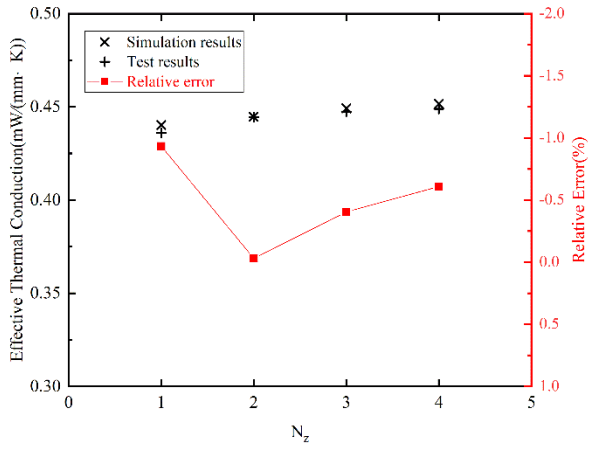

Figure 10. Relative error of the finite element model.

5.3. Validation of the prediction model

Some samples were selected to calculate the effective thermal conductivity through the finite element method. Then the prediction model was used in this study for the calculations. Then the relative error of the data was calculated and compared.

In the Tab. 2, the thermal conductivity is calculated using the finite element model. The relative errors of the traditional model and the prediction model are compared to the results of

the finite element model. It can be observed that the prediction model proposed in this paper demonstrates significantly improved accuracy compared to the traditional model.

Table 2. Comparison of relative errors of prediction models.

Sample parameters $(N_x, N_y, N_z, L_c, R, t)$	Thermal conductivity $(mW/(mm \cdot K))$	Traditional model [25] (%)	Prediction model (%)
(2,2,1,5,0.50,0.02)	0.878	16.34	0.92
(3,3,1,8,0.75,0.01)	0.266	18.66	3.82
(2,2,1,4,0.60,0.015)	0.945	40.77	9.00
(2,3,1,6,0.60,0.01)	0.367	19.64	3.80
(2,2,1,9,0.75,0.02)	0.434	13.65	1.34
(1,1,1,9,0.75,0.02)	0.472	7.76	2.61
(2,2,1,10,1.00,0.04)	0.878	16.33	0.10

6. The impact of boundary effects and structural parameters

The influence of boundary effects was compared by setting the sample at $N_z = 1$, $R = 0.75\ mm$, $t = 0.02\ mm$, $\lambda_{in} = 0.17\ Wm^{-1}K^{-1}$, $\lambda_{out} = 66.6\ Wm^{-1}K^{-1}$, and $L_c = 9\ mm$. The effective thermal conductivity was calculated with N_x and N_y being different values (Fig. 11). The prediction results of the homogenization prediction model are acceptable when the size is large enough.

When it is applied to some small devices or large-sized but not integrated, the prediction model provided in this paper should be used to obtain more accurate prediction parameters.

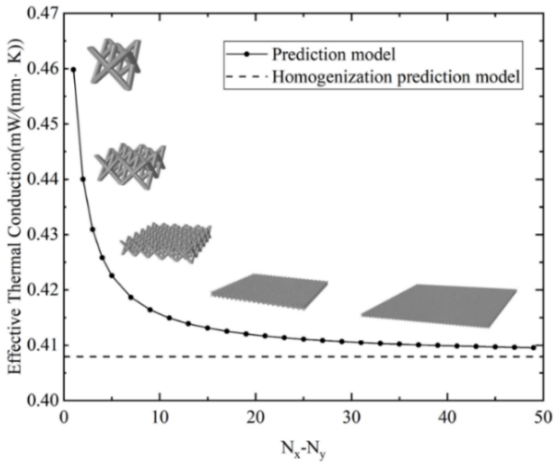

Figure 11. The impact of boundary effects.

To calculate the impact of boundary effects the conditions were set as $N_x = N_y = N_z = 1$, $\lambda_{in} = 0.17\ Wm^{-1}K^{-1}$, $\lambda_{out} = 66.6\ Wm^{-1}K^{-1}$, and $L_c = 9\ mm$. By considering the effects of R and t on the effective thermal conductivity, it can be seen from Fig. 12(a) that the tube thickness t has a greater impact than the inner radius R. This is because the thermal conductivity of the outer material is much greater than that of the inner material, which undertakes the heat transfer function, while the inner material undertakes the heat storage function. Therefore, when designing the effective thermal conductivity, the main

consideration should be given to the tube thickness t and heat transfer properties of the outer material.

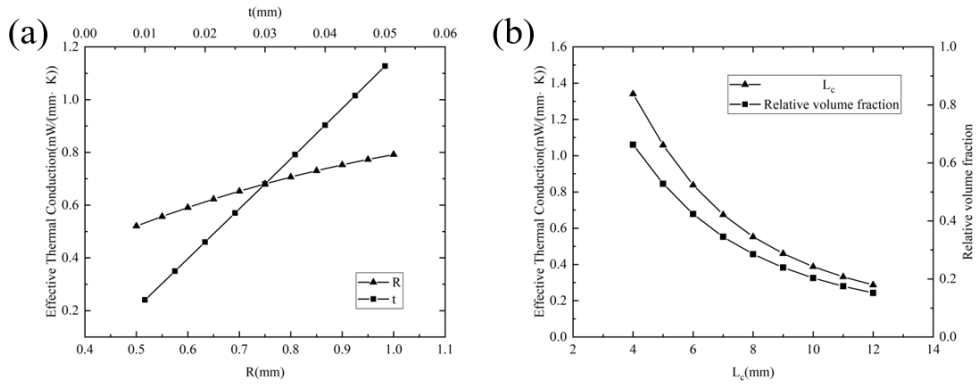

Figure 12. The impact of structural parameters.

The conditions were set at $N_z = N_y = N_z = 1$, $R = 0.75\,mm$, $t = 0.02\,mm$, $\lambda_{in} = 0.17\,Wm^{-1}K^{-1}$, and $\lambda_{out} = 66.6\,Wm^{-1}K^{-1}$. By considering the effects of L_c on the effective thermal conductivity, it can be seen that the effective thermal conductivity decreases while the L_c increases (Fig 12(b)). At the same time, it was noted that during this process, the relative volume fraction of the solid part in volume also shows the same trend and the relative volume fraction and effective thermal conductivity are linearly correlated. This is because the change in L_c does not cause a change in the intersecting parts of the structure at this time, and without considering the intersecting parts, the porosity is linearly related to the effective thermal conductivity.

In practical applications, the length of the heat transfer direction is generally determined, therefore, this parameter mainly affects the number of N_z in the heat transfer direction.

7. Conclusions

A new effective thermal conductivity prediction model for the micro-lattice phase change material in limited-size situations has been developed through theoretical models and modifications to volume formulas. The final prediction model was obtained through modification using the finite volume method. By constructing a vacuum thermal conductivity testing setup for tests and simulating with the finite element method, it was verified that the new prediction model greatly improves the accuracy compared to traditional prediction methods. In general, the accuracy of the new model has increased by 5.15%-16.23% compared to traditional models, while in some special cases where traditional models are not applicable the accuracy of the new model has increased by 30.23%.

Moreover, we compared the boundary effects under different sizes, and analyzed the impact of different structure parameters on effective thermal conductivity. The results indicate that the influence of boundary effects should not be ignored unless the size is sufficiently large. In addition, in the design of the structure, to adjust the effective thermal conductivity, the first consideration should be the thickness of the outer metal material rather than other structural parameters.

Acknowledgement

This research is supported by the National Natural Science Foundation of China (grant number: 52075326).

Nomenclature

D	Diameter of inner lattice, $[m]$
h	Interface heat transfer coefficient, $[mW mm^{-2} K^{-1}]$
k	Coefficient of fitting equation
q	Heat flux, $[mW/mm^2]$
R	Radius of inner lattice, $[mm]$
T	Temperature, $[K]$
t	Thickness of hollow tube, $[mm]$
Greek symbols	
α	Modified coefficient
λ	Thermal conductivity, $[W m^{-1} K^{-1}]$
Subscript	
c	Representative unit
p	Pole
qz	Quartz
in	Inner materials
out	Outer materials
eff	Effective parameters
s	Equivalent materials

References

[1] Zhu, L., *et al.*, Light-weighting in aerospace component and system design, *Propulsion and Power Research*, *7*. (2018), 2, pp. 103-119, DOI No. 10.1016/j.jppr.2018.04.001

[2] Nagaraju, S.B., *et al.*, *Lightweight and sustainable materials for aerospace applications*, in: *Lightweight and Sustainable Composite Materials*, (Ed., Editor^Editors. 2023, pp. 157-178.

[3] Sairajan, K.K., *et al.*, A review of multifunctional structure technology for aerospace applications, *Acta Astronautica*, *120*. (2016), pp. 30-42, DOI No. 10.1016/j.actaastro.2015.11.024

[4] Chen, J., *et al.*, Thermal control performance of phase change material combined with ultra-light hollow metallic microlattice for microsatellites, *Applied Thermal Engineering*, *227*. (2023), DOI No. 10.1016/j.applthermaleng.2023.120374

[5] Zuppardi, G., *et al.*, Aero-thermo-dynamic analysis of a low ballistic coefficient deployable capsule in Earth re-entry, *Acta Astronautica*, *127*. (2016), pp. 593-602, DOI No. 10.1016/j.actaastro.2016.06.041

[6] Cao, S.Z., *et al.*, Micro Louvers for Micro and Nano-Satellites Thermal Control, *Advanced Materials Research*, *317-319*. (2011), pp. 1658-1661, DOI No. 10.4028/www.scientific.net/AMR.317-319.1658

[7] Ashby, M.F., The properties of foams and lattices, *Philos Trans A Math Phys Eng Sci*, *364*. (2006), 1838, pp. 15-30, DOI No. 10.1098/rsta.2005.1678

[8] Sun, G., *et al.*, Low-velocity impact behaviour of sandwich panels with homogeneous and stepwise graded foam cores, *Materials & Design*, *160*. (2018), pp. 1117-1136, DOI No. 10.1016/j.matdes.2018.10.047

[9] Zhang, T., *et al.*, Toughness-improving design of lattice sandwich structures, *Materials & Design*, *226*. (2023), DOI No. 10.1016/j.matdes.2023.111600

[10] Kwak, B.-S., *et al.*, Microwave-absorbing honeycomb core structure with nickel-coated glass fabric prepared by electroless plating, *Composite Structures*, *256*. (2021), DOI No. 10.1016/j.compstruct.2020.113148

[11] Che Ghani, S.A., *et al.*, Sandwich Structure Based On Corrugated-Core: A Review, *MATEC Web of Conferences*, *74*. (2016), DOI No. 10.1051/matecconf/20167400029

[12] Xiong, J., *et al.*, Sandwich Structures with Prismatic and Foam Cores: A Review, *Advanced Engineering Materials*, *21*. (2018), 1, DOI No. 10.1002/adem.201800036

[13] Xie, B., *et al.*, Studies on the effect of shape-stabilized PCM filled aluminum honeycomb composite material on thermal control, *International Journal of Heat and Mass Transfer*, *91*. (2015), pp. 135-143, DOI No. 10.1016/j.ijheatmasstransfer.2015.07.108

[14] Wang, X., *et al.*, Thermal protection system integrating graded insulation materials and multilayer ceramic matrix composite cellular sandwich panels, *Composite Structures*, *209*. (2019), pp. 523-534, DOI No. 10.1016/j.compstruct.2018.11.004

[15] Lin, Y., *et al.*, Estimation of effective thermal conductivity in open-cell foam with hierarchical pore structure using lattice Boltzmann method, *Applied Thermal Engineering*, *218*. (2023), DOI No. 10.1016/j.applthermaleng.2022.119314

[16] Chen, K., *et al.*, A review on thermal application of metal foam, *Science China Technological Sciences*, *63*. (2020), 12, pp. 2469-2490, DOI No. 10.1007/s11431-020-1637-3

[17] Evans, A.G., *et al.*, The topological design of multifunctional cellular metals, *Progress in Materials Science*, *46*. (2001), 3, pp. 309-327, DOI No. https://doi.org/10.1016/S0079-6425(00)00016-5

[18] Torrents, A., *et al.*, Characterization of nickel-based microlattice materials with structural hierarchy from the nanometer to the millimeter scale, *Acta Materialia*, *60*. (2012), 8, pp. 3511-3523, DOI No. 10.1016/j.actamat.2012.03.007

[19] Meza, L.R., *et al.*, Strong, lightweight, and recoverable three-dimensional ceramic nanolattices, *Science*, *345*. (2014), 6202, pp. 1322-1326, DOI No. 10.1126/science.1255908

[20] Qu, Z.G., *et al.*, A theoretical octet-truss lattice unit cell model for effective thermal conductivity of consolidated porous materials saturated with fluid, *Heat and Mass Transfer*, *48*. (2012), 8, pp. 1385-1395, DOI No. 10.1007/s00231-012-0985-y

[21] Wang, X., *et al.*, Predicting the equivalent thermal conductivity of pyramidal lattice core sandwich structures based on Monte Carlo model, *International Journal of Thermal Sciences*, *161*. (2021), DOI No. 10.1016/j.ijthermalsci.2020.106701

[22] Farzinazar, S., *et al.*, Thermal transport in hollow metallic microlattices, *APL Materials*, *7*. (2019), 10, DOI No. 10.1063/1.5114955

[23] Xu, W., *et al.*, A hollow microlattice based ultralight active thermal control device and its fabrication techniques and thermal performances, *Journal of Micromechanics and Microengineering*, *32*. (2021), 1, DOI No. 10.1088/1361-6439/ac3be2

[24] Chen, J., *et al.*, Design and Analysis of a Hollow Metallic Microlattice Active Cooling System for Microsatellites, *Nanomaterials (Basel)*, *12*. (2022), 9, DOI No. 10.3390/nano12091485

[25] WADLEY, H.N.G., Multifunctional periodic cellular metals, *Philos Trans A Math Phys Eng Sci*, *364*. (2006), 1838, pp. 31-68, DOI No. 10.1098/rsta.2005.1697

[26] Li, W., *et al.*, A finite volume method for cylindrical heat conduction problems based on local analytical solution, *International Journal of Heat and Mass Transfer*, *55*. (2012), 21-22, pp. 5570-5582, DOI No. 10.1016/j.ijheatmasstransfer.2012.05.043

[27] H, W.,X.M. H, A new interpolation scheme of interface parameters for radial heat conduction, *Journal of Graduate University of Chinese Academy of Sciences*, *28*. (2011), 5, pp. 624-629

Paper submitted: 10.10.2023

Paper revised: 13.12.2023

Paper accepted: 25.12.2023